We are IntechOpen, the world's leading publisher of Open Access books Built by scientists, for scientists

6,900
Open access books available

186,000
International authors and editors

200M
Downloads

Our authors are among the

154
Countries delivered to

TOP 1%
most cited scientists

12.2%
Contributors from top 500 universities

WEB OF SCIENCE™

Selection of our books indexed in the Book Citation Index in Web of Science™ Core Collection (BKCI)

Interested in publishing with us?
Contact book.department@intechopen.com

Numbers displayed above are based on latest data collected.
For more information visit www.intechopen.com

Chapter 10

Nondestructive Tests for Induction Machine Faults Diagnosis

Paulo Cezar Monteiro Lamim Filho,
Lane Maria Rabelo Baccarini and Robson Pederiva

Additional information is available at the end of the chapter

http://dx.doi.org/10.5772/63166

Abstract

A maintenance program must include several techniques of monitoring of the electric motor's conditions. Among these techniques, probably the two classic ones are related to megger and impulse test. Unfortunately, in both cases, inherent drawbacks can expose the electrical motor at a high voltage that could deteriorate insulation condition making difficult its use on industrial environment. As the electrical machines have several different components (e.g., bearings, rotor bars, shaft, and stator windings), the fault frequencies can be excited by mechanical and/or electrical faults making the identification of the real condition difficult. This chapter describes several methods of the nondestructive tests for induction motors based on the motor current signature analysis (MCSA), magnetic flux, and vibration analysis. The method of analysis is a good alternative tool for destructive tests and fault detection in induction motors. Numerical and experimental results demonstrate the effectiveness of the proposed technique. This chapter also presents a model suitable for computer simulation of induction motor in a healthy state and with general asymmetries that can be analyzed simultaneously. The model makes it possible to conduct research on different characteristics of engines and outstanding effects produced by the faults.

Keywords: Diagnosis technique, induction motor fault diagnosis, motor current signature analysis, magnetic flux, vibration, non-destructive tests

INTECH
open science | open minds

© 2016 The Author(s). Licensee InTech. This chapter is distributed under the terms of the Creative Commons Attribution License (http://creativecommons.org/licenses/by/3.0), which permits unrestricted use, distribution, and reproduction in any medium, provided the original work is properly cited. CC BY

1. Introduction

Three-phase squirrel-cage induction motors are commonly used as electrical drives in industry because they are rugged, mechanically simple, and adaptable to a wide variety of operation conditions and simple to control.

Their design is commonly intended to have electrical and mechanical symmetries in the stator and the rotor for better coupling and higher efficiency [1]. However, the motors are exposed to different loading and environmental conditions. These conditions acting together with the natural aging of the motor may lead to many faults. The fault condition in a motor will damage the symmetrical property and induces an abnormal symptom during motor operation, such as mechanical vibration, temperature increase, irregular air-gap torque, output power variation, acoustic noise, line voltage changes, line current changes, and speed variations [1–5].

In induction electrical motors, surveys [6–9] report that the failures include internal faults (e.g., low insulation, stator interturn short circuits, worn-out/broken bearings, eccentricity, broken rotor bars, and mechanical faults) along with external faults (e.g., unbalanced supply voltage, over loading, blocked rotor, under voltage, and over voltage). These faults modify the modulation amplitudes, which are inherent in the vibration, current, and flux signals.

In order to obtain good results during the fault diagnosis of electrical machinery, a growing amount of research about new measurement instrumentation [10–13] and new signal processing techniques have been presented [14–17]. Their major goal is to improve or propose new alternative techniques to those that already exist. Among these techniques, probably the two classic ones are related to megger and impulse test. Unfortunately, in both cases, inherent drawbacks can expose the electrical motor at a high voltage that could deteriorate insulation condition making difficult their use in loco on industry plants.

An efficient and modern diagnosis technique should be nondestructive and requires only the acquisition of signals that are readily available in the motor or in the motor control center.

In the case of three-phase induction motors, which in particular represent around 85% of worldwide power consumption [18], it can be observed when using modern technologies such as the motor current signature analysis (MCSA), magnetic flux, and vibration analysis that the main faults are directly related to modulations around the power supply frequencies, rotor slot frequencies, and resonance frequencies.

This chapter describes several methods of nondestructive testing to diagnose faults of induction machine based on recent research conducted during this study. In addition, it presents a dynamic model suitable for computer simulation of induction machines in a healthy state with general asymmetries, such as power systems unbalance, stator interturn short circuit, rotor broken bars, and mechanical faults. The model is an important tool of new diagnostic techniques project because it provides analysis of the impact of failures on the characteristics of the electrical machinery.

This chapter is organized as follows. The dynamic model and the characteristic frequencies of the faults are presented in Section 2. A sound knowledge of dynamic model and characteristic

http://dx.doi.org/10.5772/63166

frequencies will facilitate understanding the health condition of the electrical machine. The simulation and experimental results are described in Section 3. Finally, conclusions are presented in Section 4.

2. Fault models

The symmetrical machine model is well known in the literature. The dynamic model proposed by Baccarini et al. [19] accounts for both mechanical and electrical faults in induction machines. The model allowed several simulations in different conditions and outstanding effects produced by the faults. The asymmetries can be power systems unbalance, stator interturn short circuit, rotor broken bars, and mechanical faults (unbalance, misalignment, and mechanical looseness). A convenient selection of the state-space variable set enables description of the machine with a very simple set of equations. The model is described in Section 2.1. To facilitate understanding of the relationship failure/sign, the characteristic frequencies of the faults are described in Section 2.2.

2.1. Dynamic model

2.1.1. Unbalance supply voltage

Unbalance supply voltage is characterized by the nonequality of voltage magnitudes and/or when voltage angles among the three phases are different of $2\pi/3$. In this chapter, the voltage unbalance is represented by Eqs. (1)–(3), where w is the angular velocity and the subscript "s" denotes variables and parameters associated with the stator circuits. When the voltage is balanced the values K_{as}, K_{bs}, and K_{angle} are unities:

$$v_{as} = K_{as} V_{\max} \cos(wt), \tag{1}$$

$$v_{bs} = K_{bs} V_{\max} \cos\left(wt - K_{angle} \frac{2\pi}{3}\right), \tag{2}$$

$$v_{cs} = -(v_{as} + v_{bs}). \tag{3}$$

A change of variables that formulates a transformation of the three-phase variables of the machine circuits to two-phase transformation is given by Eqs. (4)–(6):

$$\left[f_{dq}\right] = K_s\left[f_{abs}\right], \tag{4}$$

$$\begin{bmatrix} f_q \\ f_d \\ f_0 \end{bmatrix} = \frac{2}{3}\begin{bmatrix} \cos\theta & \cos\left(\theta - \frac{2\pi}{3}\right) & \cos\left(\theta + \frac{2\pi}{3}\right) \\ \sin\theta & \sin\left(\theta - \frac{2\pi}{3}\right) & \sin\left(\theta + \frac{2\pi}{3}\right) \\ \frac{1}{2} & \frac{1}{2} & \frac{1}{2} \end{bmatrix}\begin{bmatrix} f_a \\ f_b \\ f_c \end{bmatrix}, \tag{5}$$

$$\theta = \int_0^t w(\varepsilon)\, d\varepsilon + \theta_0, \tag{6}$$

where f represents either voltage, current, flux linkage, or electric charge. The variable ε is a dummy variable of integration.

2.1.2. Symmetric model

The voltage v, the flux λ, and the current i can be expressed in arbitrary reference frame. The equations for the stator and rotor flux are expressed as

$$\frac{d\lambda_{qs}}{dt} = v_{qs} - r_s i_{qs} - w\lambda_{ds}, \tag{7}$$

$$\frac{d\lambda_{ds}}{dt} = v_{ds} - r_s i_{ds} + w\lambda_{qs}, \tag{8}$$

$$\frac{d\lambda_{qr}}{dt} = -r_r i_{qr} - \left(w - w_r\right)\lambda_{dr}, \tag{9}$$

$$\frac{d\lambda_{dr}}{dt} = -r_r i_{dr} + \left(w - w_r\right)\lambda_{qr}. \tag{10}$$

The subscript "r" indicates the variables, the parameters, and the transformation associated with rotor circuit. The machine electromagnetic torque T_e, the load torque T_{load}, and the rotor velocity w_r are related as

http://dx.doi.org/10.5772/63166

$$\frac{dw_r}{dt} = \frac{T_e - B_m w_r - T_{load}}{J}, \tag{11}$$

where J is the combined moment of inertia of the motor and the mechanical load. The constant B_m represents the viscous friction associated with the mechanical load and motor.

The Runge–Kutta fourth-order method is used to obtain the solution to the differential equations expressed in (7)–(11).The currents of the stator and the rotor are represented by Eqs. (12)–(15):

$$i_{qs} = \lambda_{qs} a_1 - \lambda_{qr} a_2, \tag{12}$$

$$i_{ds} = \lambda_{ds} a_1 - \lambda_{dr} a_2, \tag{13}$$

$$i_{qr} = \lambda_{qr} a_3 - \lambda_{qs} a_2, \tag{14}$$

$$i_{dr} = \lambda_{dr} a_3 - \lambda_{ds} a_2, \tag{15}$$

where $a_0 = L_s L_r - L_m^2$; $a_1 = \frac{L_r}{a_0}$; $a_2 = \frac{L_m}{a_0}$; $a_3 = \frac{L_s}{a_0}$.

The parameters L_s and L_r are the stator and rotor self-inductances, and L_m is the mutual inductance. The expression for the electromagnetic torque in terms of arbitrary reference frame for a p-pole machine may be expressed as

$$T = \frac{3}{2}\frac{p}{2}\left(\lambda_{ds} i_{qs} - \lambda_{qs} i_{ds}\right). \tag{16}$$

2.1.3. Mechanical fault model

The occurrence of motor mechanical faults (unbalance, misalignment, and mechanical looseness) results changes in the air-gap space harmonics distribution, which leads to a sideband currents in the current spectrum that can be written as

$$f_{mec} = f\left(1 \pm K_{mec}\frac{1-s}{p}\right), \tag{17}$$

where f is the stator supply frequency, K_{mec} = 1, 2, 3, … is the order number, and s represents the motor slip. The slip is defined as

$$s = \frac{w - w_r}{w}. \tag{18}$$

The interaction of those harmonics with the mainly sinusoidal supply voltage causes specific harmonics in the power and torque spectrum:

$$f_{torque} = K_{torque} \frac{1-s}{p}. \tag{19}$$

Considering the harmonics in torque spectrum, the mechanical faults are analyzed, in this model, by introducing a load torque modulation T_{mec} associated with the rotation frequency in the load torque. Thus, Eq. (11) becomes

$$\frac{dw_r}{dt} = \frac{T_e - B_m w_r - T_{load} - T_{mec} \sin\left(2\pi f_s t\right)}{J}. \tag{20}$$

2.1.4. Stator fault model

The shorted turns leakage inductance is assumed to be μL_{ls} where μ denotes the shorted turns fraction. The voltage v andd flux linkage λ equations of the stator and rotor windings are transformed to dq axes, rotating at an arbitrary speed $w = d\theta / dt$. The machine stator equations can be expressed in complex two-phase dq variables as follows:

$$\frac{d\lambda_{qs}}{dt} = v_{qs} - r_s i_{qs} - w\lambda_{ds} + \frac{2}{3}\mu r_s i_f \cos\theta, \tag{21}$$

$$\frac{d\lambda_{ds}}{dt} = v_{ds} - r_s i_{ds} + w\lambda_{qs} + \frac{2}{3}\mu r_s i_f \sin\theta. \tag{22}$$

The equations for rotor circuits are equal to those corresponding to a healthy motor as in Eqs. (9)–(10). For the shorted turns, the flux linkage equation is

$$\frac{d\lambda_{as2}}{dt} = r_f i_f - \mu r_s \left(i_{ds}\cos\theta + i_{qs}\sin\theta - i_f\right), \tag{23}$$

where r_f and i_f represent the fault resistance and the short-circuit current, respectively.

http://dx.doi.org/10.5772/63166

The stator and rotor currents are obtained from the following equations:

$$i_{qs} = \lambda_{qs} a_7 - \lambda_{qr} a_8 + \left(L_r a_{10} - L_m a_{11}\right) i_f \cos\theta, \tag{24}$$

$$i_{ds} = \lambda_{ds} a_7 - \lambda_{dr} a_8 + \left(L_r a_{10} - L_m a_{11}\right) i_f \sin\theta, \tag{25}$$

$$i_{qr} = \lambda_{qr} a_9 - \lambda_{qs} a_8 + \left(L_s a_{11} - L_m a_{10}\right) i_f \cos\theta, \tag{26}$$

$$i_{dr} = \lambda_{dr} a_9 - \lambda_{ds} a_8 + \left(L_s a_{11} - L_m a_{10}\right) i_f \sin\theta, \tag{27}$$

$$i_f = \left[-\lambda_{as2} + \left(a_{12} i_{qs} + a_{13} i_{qr}\right)\cos\theta + \left(a_{12} i_{ds} + a_{13} i_{dr}\right)\sin\theta\right] / a_{14}, \tag{28}$$

where $a_6 = 1 - \frac{L_m^2}{L_s L_r}$; $a_7 = \frac{1}{a_6 L_s}$; $a_8 = \frac{L_m a_7}{L_r}$; $a_9 = \frac{1}{a_6 L_r}$; $a_{10} = \frac{2}{3}\frac{\mu L_s}{a_0}$; $a_{11} = \frac{2}{3}\frac{\mu L_m}{a_0}$;
$a_{12} = \mu L_s$; $a_{13} = \mu L_m$; $a_{14} = \mu\left(L_s + \frac{2}{3}\mu L_m\right)$.

The electromagnetic torque is expressed in dq variables as shown in Eq. (29): the first member of this equation is equal to those corresponding to a healthy motor and the second member is the additional component introduced by the fault:

$$T = \frac{3}{2}\frac{p}{2} L_m \left(i_{qs} i_{dr} - i_{ds} i_{qr}\right) + \frac{p}{2} \mu L_m i_f \left(i_{qr} \sin\theta - i_{dr} \cos\theta\right). \tag{29}$$

2.1.5. Rotor fault model

The rotor fault model is proposed by Cunha et al. [20]. The complex vector rotor current, Eq. (15) or Eqs. (26) and (27), is computed from the symmetric model in rotor-fixed reference frame as in Eq. (30). The T_{dq} transformation matrix is generated by a simple algorithm, Eq. (31):

$$\begin{bmatrix} i_{r1} \\ i_{r2} \\ \vdots \\ i_{rn} \end{bmatrix} = T_{dq}^{-1} \begin{bmatrix} i_{dr} \\ i_{qr} \\ \vdots \\ i_0 \end{bmatrix}, \tag{30}$$

$$T_{\mathrm{dq}} = K_{\mathrm{b}} \begin{bmatrix} \cos\theta & \cos\left(\theta - \frac{p}{2}\frac{2\pi}{n}\right) & \cos\left(\theta - \frac{p}{2}\frac{4\pi}{n}\right) & \cos\left(\theta - \frac{p}{2}\frac{n-1}{n}2\pi\right) \\ \sin\theta & \sin\left(\theta - \frac{p}{2}\frac{2\pi}{n}\right) & \cos\left(\theta - \frac{p}{2}\frac{4\pi}{n}\right) & \sin\left(\theta - \frac{p}{2}\frac{n-1}{n}2\pi\right) \\ f_{31} & f_{32} & 1 & 0 \\ f_{41} & f_{42} & 0 & 0 \\ f_{n1} & f_{n2} & 0 & 1 \end{bmatrix}, \tag{31}$$

where $K_{\mathrm{b}} = \frac{n-1}{n}$.

It is known that the fault current is mainly divided in a few bars adjacent to the broken bar. Considering that the bar kth is broken, the zero current through this bar is achieved by changing the n-loop rotor current as in Eq. (32). Finally, the new n-dimensional rotor current vector is determined by Eq. (33) and fed back to the induction motor integration algorithm;

$$\begin{bmatrix} i_{r1}^{new} \\ i_{r2}^{new} \\ \cdots \\ i_{rk}^{new} \\ i_{r(k+1)}^{new} \\ \cdots \\ i_{rn} \end{bmatrix} = \begin{bmatrix} i_{\mathrm{r}1} \\ i_{\mathrm{r}2} \\ \cdots \\ \frac{i_{\mathrm{r}k} + i_{\mathrm{r}(k+1)}}{2} \\ \frac{i_{\mathrm{r}k} + i_{\mathrm{r}(k+1)}}{2} \\ \cdots \\ i_{\mathrm{r}n} \end{bmatrix}, \tag{32}$$

$$\begin{bmatrix} i_{rd}^{new} \\ i_{rq}^{new} \\ i_{01} \\ i_{0k} \\ i_{0(k+1)} \\ \cdots \\ i_{0r} \end{bmatrix} = \begin{bmatrix} i_{r1}^{new} \\ i_{r2}^{new} \\ \cdots \\ i_{rk}^{new} \\ i_{r(k+1)}^{new} \\ \cdots \\ i_{rn}^{new} \end{bmatrix}. \tag{33}$$

2.1.6. Complete model

Figure 1 shows the flowchart of the computer program that is suitable for computer simulation of induction machines in a healthy state with general asymmetries: power systems unbalance,

http://dx.doi.org/10.5772/63166

stator interturn short circuit, rotor broken bars, and mechanical faults. The parameters t and h are the total simulation and integration time values in seconds.

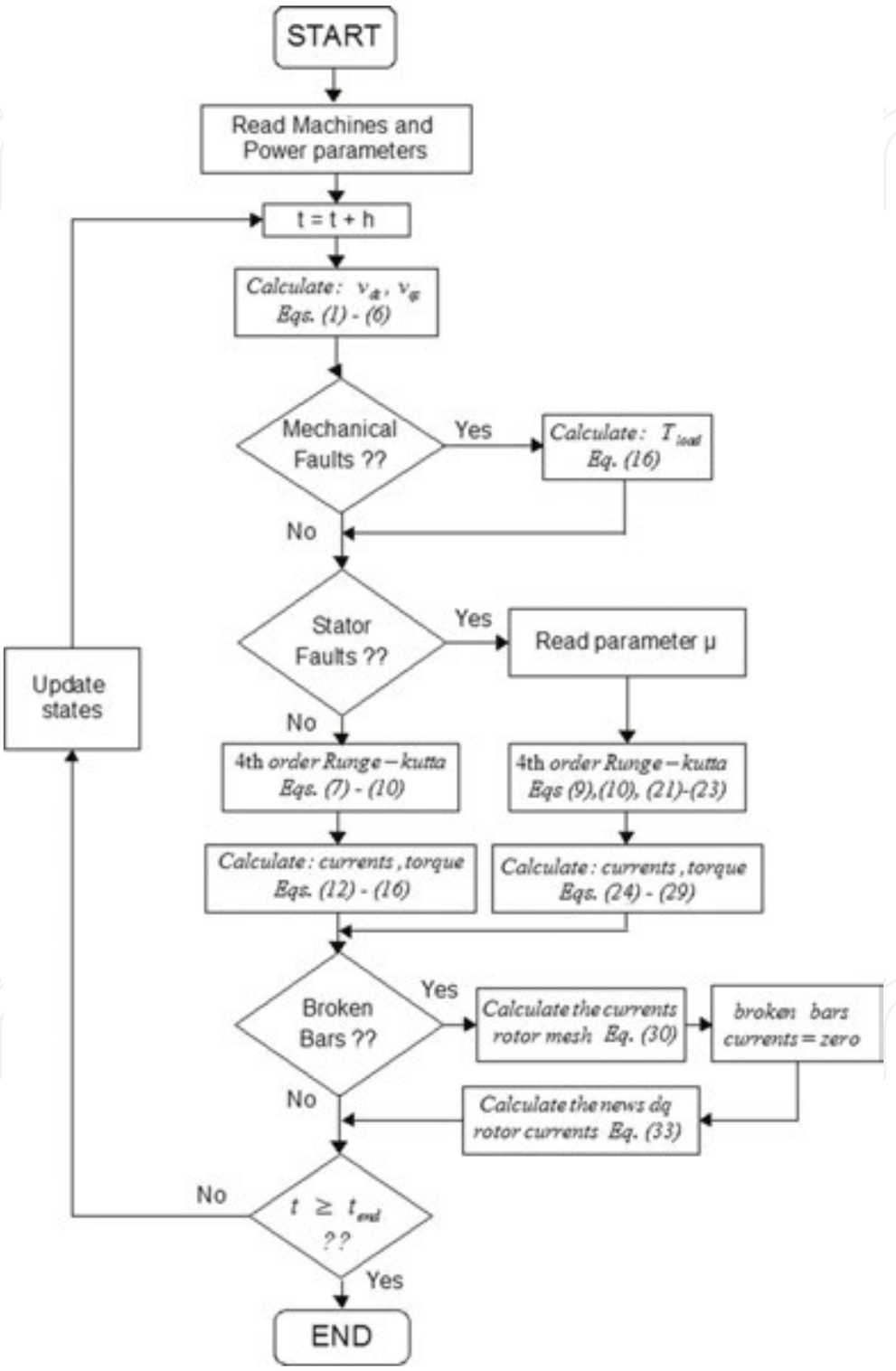

Figure 1. Flowchart of the computer program.

2.2. Characteristic frequencies of faults

2.2.1. Unbalance supply voltage

The study of the rotating magnetic field nature presented here is important to give a better understanding of the deterministic frequencies identification related to the unbalanced voltage supplies, using vibration and magnetic flux analysis.

The three-phase induction motor, composed by stator and rotor, usually works at the constant speed, but small changes can occur due to changes of the mechanical load linked to the shaft.

The stator is composed of laminations of high-grade steel sheet. A three-phase winding is put in slots cut on the inner surface of the stator frame. The rotor also consists of laminated ferromagnetic material, with slots cut on the outer surface.

The squirrel-cage windings consists of aluminum or copper bars embedded in the rotor slots and shorted at both ends by aluminum or copper end rings. The three-phase winding on the stator is a distributed winding. The winding of each phase is distributed over several slots. When current flows through a distributed winding it produces a sinusoidal distributed magnetomotive force (MMF) centered on the axis of the coil representing the phase winding. If an alternating current flows through the coil, it produces a pulsating MMF wave, whose amplitude and direction depend on the instantaneous value of the current flowing through the windings.

The definition of unbalanced voltage used by the power community is the ratio of the negative sequence voltage to the positive sequence voltage [21]. For a set of unbalanced voltages V_{ab}, V_{bc}, and V_{ca}, the positive and negative sequence voltages are given by

$$V_{ab1} = \frac{V_{ab} + aV_{bc} + a^2V_{ca}}{3}, \tag{34}$$

$$V_{ab2} = \frac{V_{ab} + a^2V_{bc} + aV_{ca}}{3}, \tag{35}$$

where $a = -0.5 + j0.855$, $a^2 = -0.5 + j0.855$, and V_{ab1} and V_{ab2} are positive and negative phase sequences, respectively.

Each set produces corresponding balanced currents, and two vectors represent the three-phase currents of the stator.

The positive sequence voltage is the same as for machine in a regular operation condition. However, the negative sequence will produce a reverse rotating field and the slip rotor will be $2 - s$. The motor behaves as the addition of two separate motors, one running at slip s with a terminal voltage of V_{ab1} per phase and the other running with a slip of $2 - s$ and a terminal voltage of V_{ab2}.

http://dx.doi.org/10.5772/63166

The frequency of the induced rotor voltage for this negative motor is approximately 120 Hz. This high frequency in the rotor causes the rotor current to concentrate in the top of the rotor conductors, thus increasing the effective rotor resistance and decreasing the effective rotor leakage reactance. The increase in the effective rotor resistance reflects a significant increase in rotor losses I^2R for a given value of rotor current [22].

Unbalance supply voltage is a usual industrial problem that generates electrical machine overheating, reducing lifetime, provoking vibration that thereafter generates mechanical wear, and noise.

The influence of voltage unbalance upon three-phase induction motors has long been a concern of electrical engineers. One of the main scopes of this chapter is about nondestructive test on the induction motor under voltage unbalance. The paper [21] reviews three definitions of voltage unbalance developed by NEMA, IEEE, and the power community, respectively. The differing definitions of voltage unbalance are analyzed in order to understand the implications of their use.

2.2.2. Short circuit

The presence of interturn short circuit and/or unbalanced voltage supply will give rise to a magnetic asymmetry that crosses the machine's air gap. These asymmetry can result in magnetizing current proportional to the rotor slot harmonic frequencies and their respective modulations in twice the line frequency, i.e., $(1 \pm \lambda n(1 - s)/p)fl \pm 2fl$, $\pm 4fl$, etc., where $\lambda = 1, 2, 3, \ldots$, n is the number of rotor bars or slot, p is the number of pole pairs, fl is the line frequency, and s is the rotor slip. These frequencies of stator current will generate a torque pulsation and consequently vibration that is transmitted through the motor frame. These considerations are based on studies conducted by Gojko and Penman [23] and Gupta and Culbert [24], for three-phase motor.

3. Nondestructive diagnostic method

Using the model described in Section 2.1, several analyses were performed and fault diagnosis algorithms were developed by Baccarini et al. [19,26]. The proposed methods allow the full engine diagnostics, i.e., verify the absence or the presence of the following failure conditions: initial short-circuit, broken bars, and mechanical failures.

The proposed methods were validated on a test bench. The results and the test bench are described in Section 3.1. The methods are nondestructive and need only the information of the current sensors, typically present in an industrial plant. Therefore, these techniques will be referred to herein, "the signal current methods."

The results and experimental analysis of Sections 2.2.1 and 2.2.2 are described in Section 3.2.

3.1. The signals current methods

3.1.1. Description of the experimental setup 1

The experimental system is set with special induction machine to simulate the failure, a direct current (dc) machine, a measuring system, encoder, computer, a three-phase varivolt, resistances, and the board acquisition.

A separate dc generator feeding a variable resistor provides a mechanical load. In order to allow tests to be performed at different load levels, the dc excitation current and load resistor are both controllable.

The motor was rewound to allow short-circuit simulation between different numbers of coil turns. The stator windings are connected in delta in all tests. In order to prevent damage of the stator windings, a resistor was used to limit the short-circuit current.

Either the mechanical structure where the motors are settled offers the possibility to move the two machines, in a way the system can be aligned or different degrees of misalignment can be tested. Shaft alignment in the setup was guaranteed by using a laser alignment tool.

The motor was initially set with the cage intact and several tests were realized with the symmetric rotor. The rotor bar fault has been caused by drilling holes into the aluminum bars.

3.1.2. Winding short-circuit fault and unbalance supply voltage

To validate the proposed method, simulations of different induction machine were carried out. The simulations presented here refer to a motor with the following nominal parameters: 3 CV, 220 V, 60 Hz, 4 poles, and 1710 rpm. It is the motor of the test bench. The Monte Carlo computational algorithm was used to simulate random motor operation conditions: mechanical load, different broken bar, degree of mechanical fault, different percentages of turns shorted, level of voltage unbalance, and noise in the measurement system.

Several experimental results are presented below to demonstrate the robustness and accuracy of the stator short-circuit model. The negative sequence impedance of a healthy induction motor is practically constant. However in the presence of short-circuit failure, the symmetry of the windings is lost and the value of negative impedance changes.

Multiple experimental tests were performed on different days and times. The negative sequence impedances for each test were calculated. The average value of impedance is the situation of lack of failures. Other series of tests were performed in the following conditions: the absence of short circuit with 3, 6, and 15 shorted turns. **Figure 2** shows the mean and square mean error of the negative components impedance for a healthy motor with 3, 6, and 15 shorted turns.

Results from the experiments are very encouraging. The performance was not affected by the voltage supply unbalances or inherent machine and/or monitoring system asymmetry. It can be seen that experimental results exhibit the same trend as predicted by the model.

http://dx.doi.org/10.5772/63166

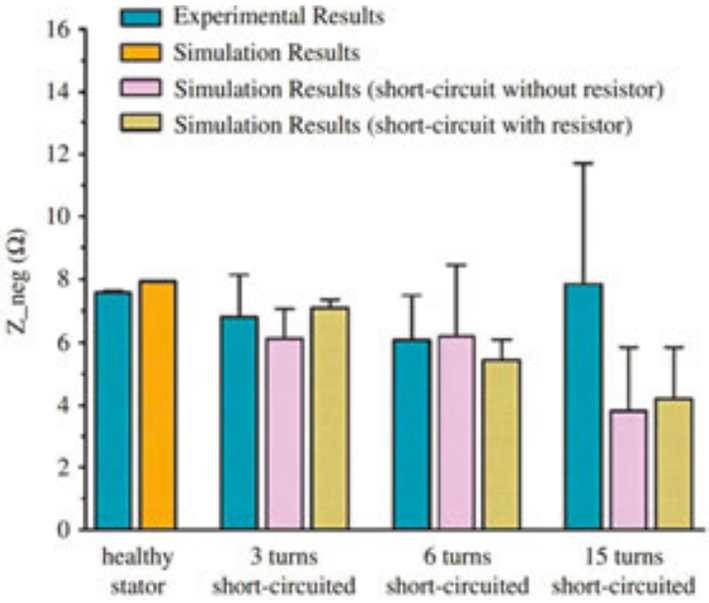

Figure 2. Mean and square mean error of the negative component impedance for healthy motor with 3, 6 and 15 shorted turns.

3.1.3. Mechanical faults

The presence of mechanical fault is analyzed in simulation and experimental tests. **Figure 3a** and **b** shows the simulation stator current spectrum of the motor with different levels of mechanical failures and operation at rated load. The nominal load frequency f_r is 28.5 Hz. In that way, the spectrum contains components near 31.5 and 88.5 Hz. These $f \pm f_r$ components point out the presence of mechanical fault and their amplitudes increase as the mechanical fault's level rises.

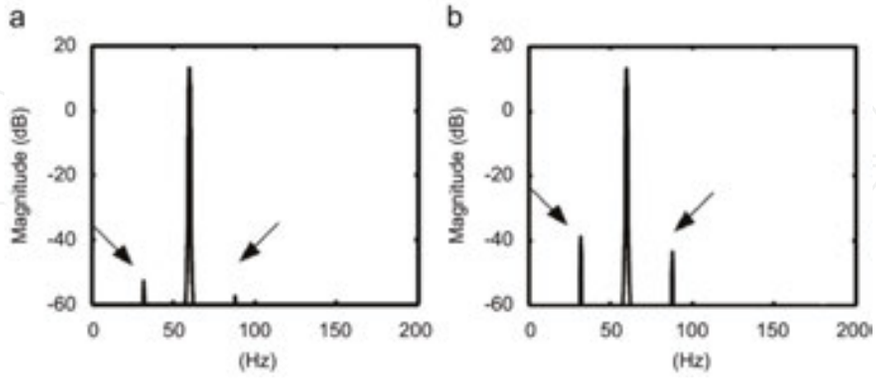

Figure 3. Simulation current frequency spectrum.

Figure 4 shows the phase current spectra for a motor with mechanical fault. The zoom spectra are centered on the fundamental frequency (60 Hz). The component 32 Hz ($f - f_r$) and the component 88 Hz ($f + f_r$) indicates the presence of mechanical fault.

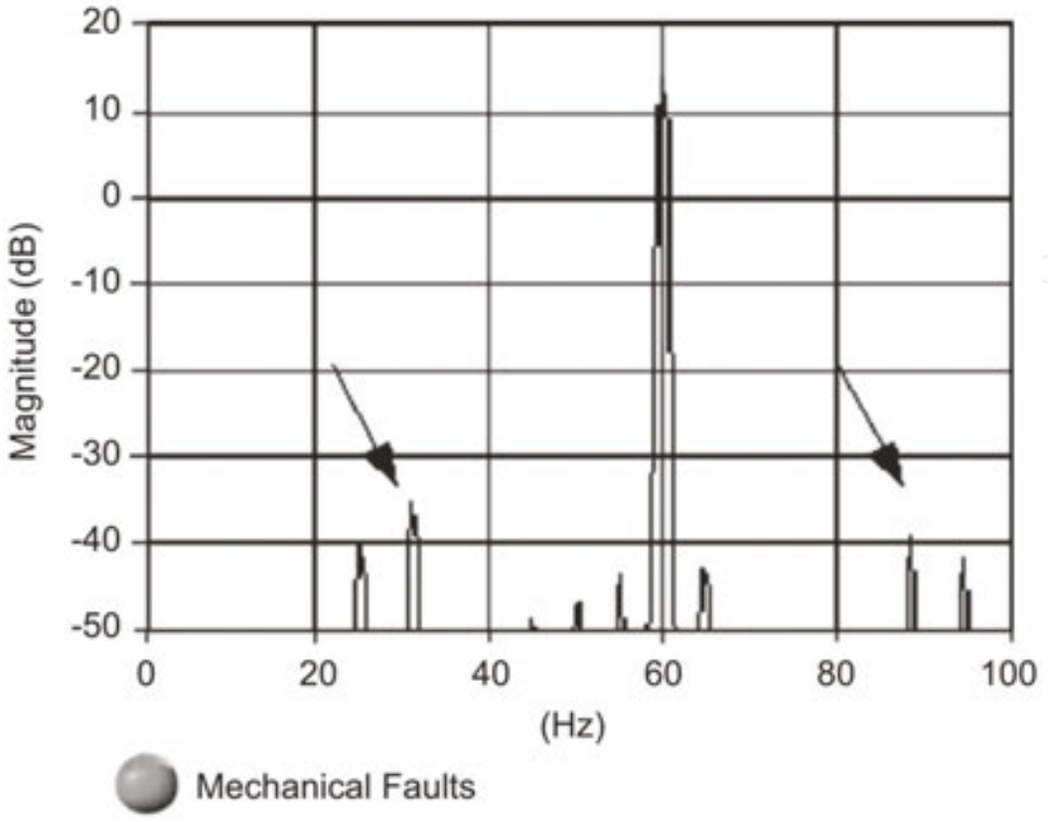

Figure 4. Experimental current frequency spectrum and mechanical faults.

3.1.4. Broken rotor bars

The best-known technique for the detection of broken bars in induction motors is related to monitoring the side bands around the fundamental frequency of the stator current. However, the stator current is a nonstationary signal as it changes over time. Therefore, the fault rotor bar detection using the frequency spectrum is a difficult task that needs a complex signal processing.

The Vienna Monitoring Method (VMM) was proposed for diagnosing faults in the rotor cage induction motors. The technique estimates the torque of induction machine using two different models: voltage model (T_v) and current model (T_c) [25]. In symmetric rotor condition, no faults, the difference torque between the two models ($\Delta T = T_v - T_c$) is almost zero. In the case of a rotor failure, the resultant torque ΔT oscillates at twice the slip frequency.

Baccarini et al. [26] also proposed a method for online monitoring of the induction motor in order to detect and locate a single broken rotor bar. Similar to the VMM, the technique does not use the frequency spectrum. The machine states are calculated with the help of two models. One model is designed to reject asymmetries in the rotor resistance. The other estimates the rotor flux using the discrete model proposed by Bottura et al. [27]. The presence of asymmetry in the rotor causes a different response in the form of a modulated torque deviation. The

http://dx.doi.org/10.5772/63166

frequency of the modulation is determined by two times the slip frequency. A minimum of torque difference indicates the faulty rotor bar location.

3.1.4.1. Simulations results

Figure 5 shows the torque modulation, simulation results, for three load operating conditions (112, 78, and 45% of nominal load). The presence of broken rotor bars results in the presence of a noticeable deviation in the torque's magnitude. The torque residue has a constant term and an oscillating term that is related to the presence of broken bars.

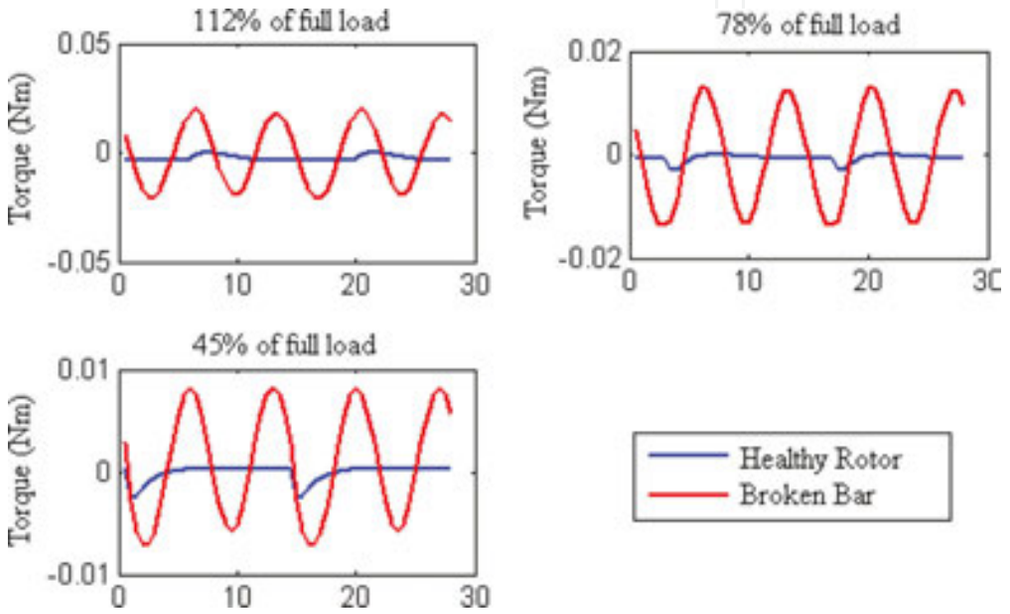

Figure 5. Induction motor torque deviation for healthy rotor and one broken rotor bar for three different load operating conditions and simulations results.

3.1.4.2. Experimental results

Several tests were performed to obtain the torque residue for a healthy rotor for different load operating conditions. **Figure 6** shows the torque residue for a healthy rotor. The value of the maximum residue gives the fault pattern. The presence of these residues is probably due to inherent rotor asymmetries.

The fault of the rotor bar has been caused by drilling a hole in an aluminum bar of a genuine motor and several tests were performed by different load conditions. The torque residues are shown in **Figure 7a** and **b** for nominal and 60% of nominal load condition. Due to the presence of broken bars, these values are higher than the reference standard (**Figure 6**). The modulation frequency is twice the slip frequency. For operation with low load (**Figure 7b**), the modulation frequency is lower compared to the nominal operating conditions (**Figure 7a**), as a result of the low value of the slip. The fault diagnosis is not compromised because of the low value of

slip. The technique allows the diagnosis of the presence of cracks or broken bars for all operating conditions.

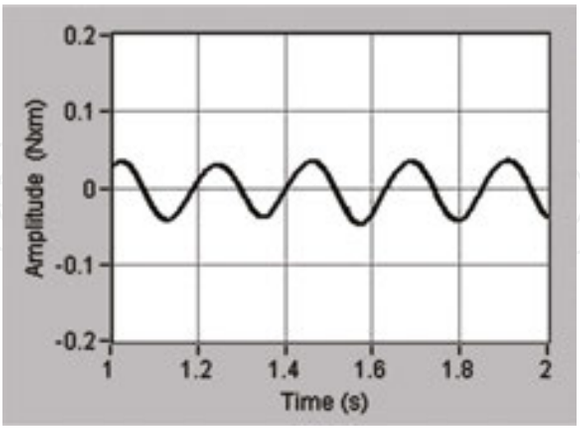

Figure 6. Full load motor operating condition torque residue for healthy rotor, fixed as pattern fault. Experimental results.

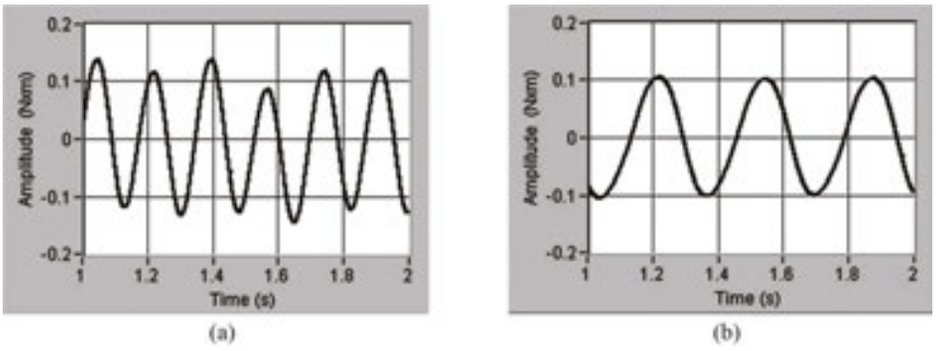

Figure 7. Torque residue for one broken rotor bar; experimental results: (a) full load motor operating condition; (b) 60% nominal load motor operating condition.

3.2. Characteristic frequencies analysis

3.2.1. Description of the experimental setup 2

The experimental systems is set with special three-phase induction motor to simulate the faults, 5 HP, 1730 rpm, 220 V, 13.8 A, 60 Hz, 4 poles, 44 bars, and 36 slots. A dc generator feeding a resistance bank is used as a load system. By varying the excitation current of the dc generator field and therefore its output voltage, a variation of the motor load can be obtained [11, 28].

A torque meter, 0–7500 rpm, bidirectional, and maximum toque of 1000 LB-IN was used to ensure the same operating conditions in all tests. To simulate a low isolation, among turns from the same phase four tappings in a coil were extracted and this makes possible the control of the turns in short circuit.

http://dx.doi.org/10.5772/63166

The flux signals were acquired by a magnetic flux sensor [11]. The vibration signals were acquired by an accelerometer, sensitivity 10.13 mV/g, and frequency range from 1 Hz to 20 kHz. It was observed from the spectra of vibration that all tests had a good repeatability and that there were no variations of mechanical origin that would interfere in the spectra of vibration, ensuring a perfect analysis of the results**.**

Magnetic flux and vibration signals were collected (total of 300) from a series of 10 tests at each excitement (without fault, two, four, and eight turns short circuits, and voltage unbalance) and randomly repeated under the same load conditions (100, 90, and 80% of load).

The signs of magnetic flux and vibration were submitted to an antialiasing filter with 2.5 kHz of cut frequency and 5 kHz of sampling frequency.

3.2.2. Magnetic flux and vibration

The main rotor slot frequencies and their side bands described in Section 2.2.1 and 2.2.2 are computed at $\lambda = 1$, $n = 44$, $s = 0.036$, $p = 2$, and $fl = 60$ (1212.48 and 1332.48 Hz). The spectra computed by FFT for the magnetic flux and vibration in linear scale with the motor working without fault and full load are shown in **Figure 8**. Unlike the vibration spectrum, the magnetic flux spectrum clearly shows the frequencies 1212.48 and 1332.48 Hz. This is because the magnetic flux signals have a strong presence of the rotor slot frequencies and their side bands [28].

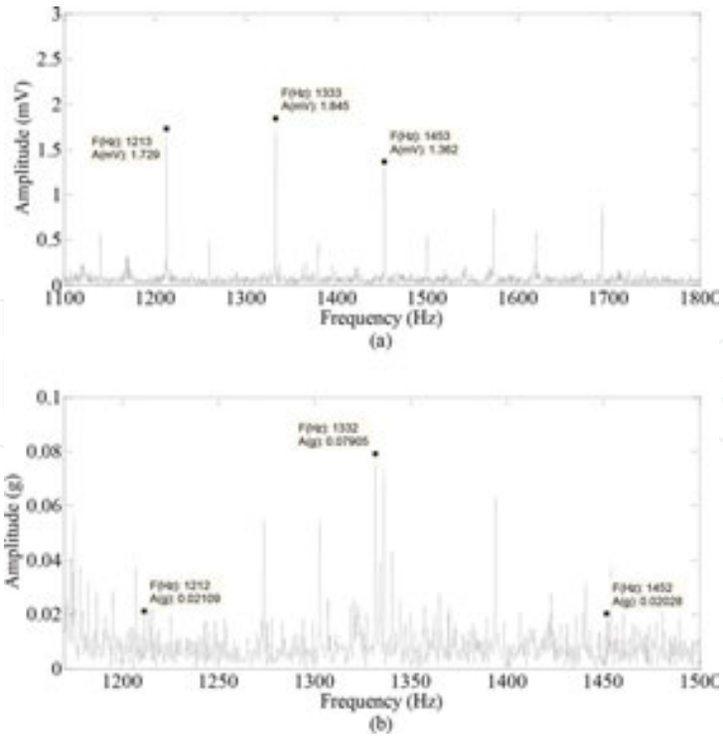

Figure 8. Spectra without fault, with machine operating at nominal speed, and under full load: (a) magnetic flux; (b) vibration.

The visualization of the components of rotor slot harmonic frequencies, **Figure 8**, that had been most excited by the short circuit and voltage unbalance imperfections turns out to be extremely difficult.

Given this difficulty, Lamim Filho et al. [11] have proposed the application of the envelope analysis by Hilbert transform (HT) [29], which is very used in the detection of mechanical faults, for the visualization of the rotor slot frequency components that have been most excited by the electrical faults.

Thus, by applying Hilbert transform in the frequency range from 1 to 2 kHz for magnetic flux and vibration analysis, low-frequency flux and vibration spectra were obtained in which the rotor slot frequency components became extremely easy to visualize and compare with each other.

The spectra of the magnetic flux and vibration after the application of envelope analysis for the motor working at a full-load condition without fault, short circuit of eight turns, and voltage unbalanced *(*V_{ab} = 200 V, V_{bc} = 200 V, and *V*ca = 220 V*)* are shown in **Figures 9** and **10**, respectively.

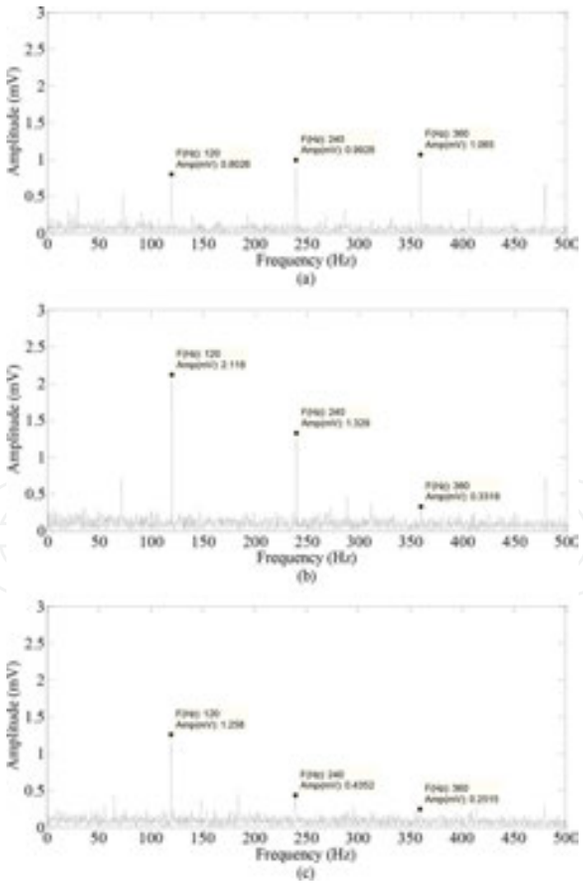

Figure 9. Envelope analysis from the flux magnetic signal with machine operating at nominal speed and full load: (a) without fault; (b) eight turns short-circuited (c) voltage unbalance 200 V.

http://dx.doi.org/10.5772/63166

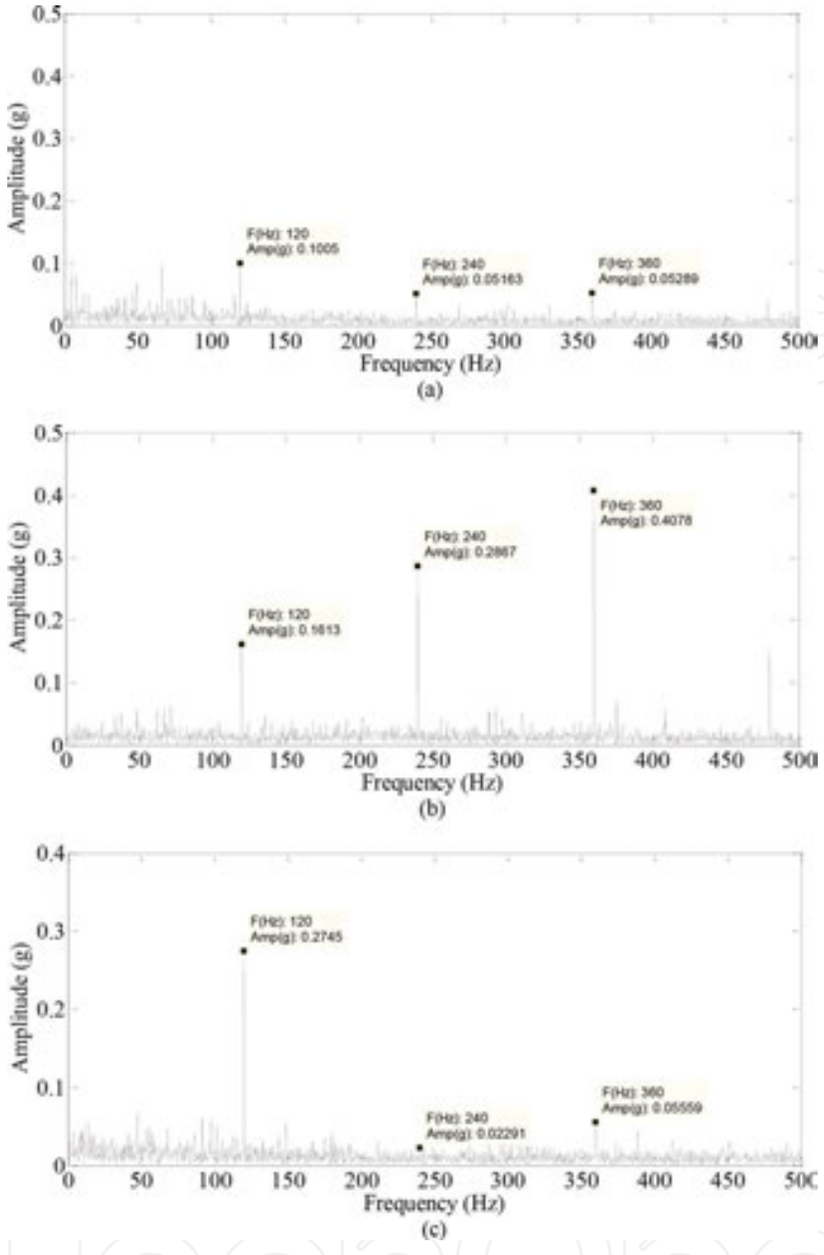

Figure 10. Envelope analysis from the vibration signal with machine operating at nominal speed and full load: (a) without fault; (b) eight turns short-circuited (c) voltage unbalance 200 V.

After comparing the spectra of the magnetic flux signals and the spectra of the vibration signals, it could be verified that the components of frequency demodulated in 2*fl* (120 Hz), 4*fl* (240 Hz), and 6*fl* (360 Hz) were excited the most by the insertion of the short circuit and voltage unbalanced (Figures 10 and 11). Therefore, these harmonics will be considered as the characteristic frequencies for the identification of short circuit and voltage unbalanced, and will be referred to as second (2dh), fourth (4dh), and sixth demodulated harmonic (6dh). For the magnetic flux and vibration analysis, the graphs of tendency for the motor working with 100, 90, and 80% of load are shown in **Figures 11** to **13**, respectively.

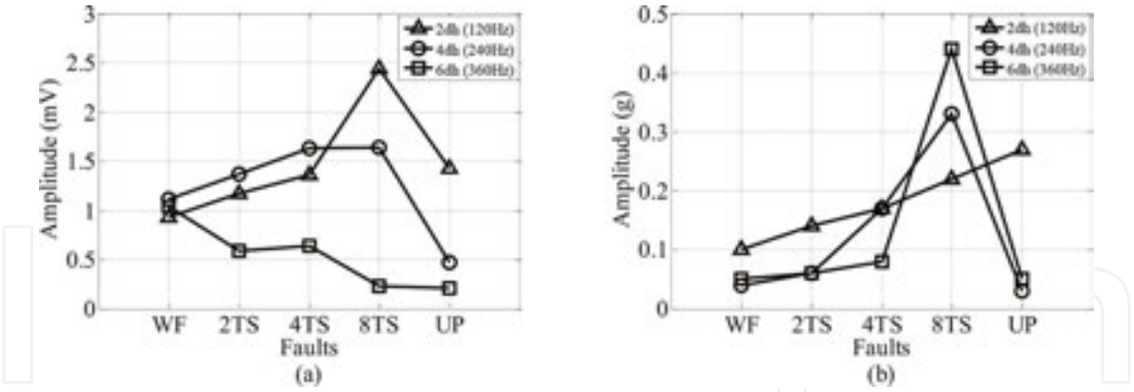

Figure 11. Tendency of the faults introduced into the motor with 100% of load, without fault (WF), two turns short (2TS), four turns short (4TS), eight turns short (8TS), and voltage unbalanced (UP): (a) magnetic flux; (b) vibration.

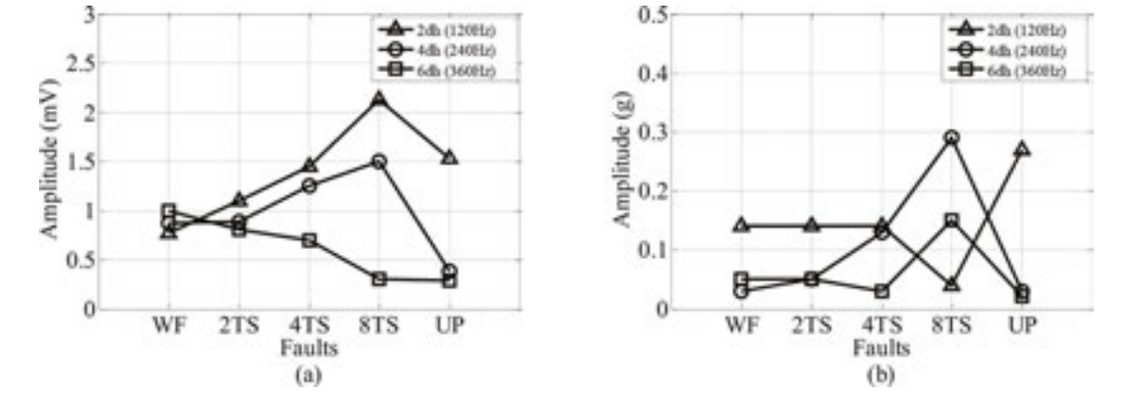

Figure 12. Tendency of the faults introduced into the motor with 90% of load, without fault (WF), two turns short (2TS), four turns short (4TS), eight turns short (8TS) and voltage unbalanced (UP): (a) magnetic flux; (b) vibration.

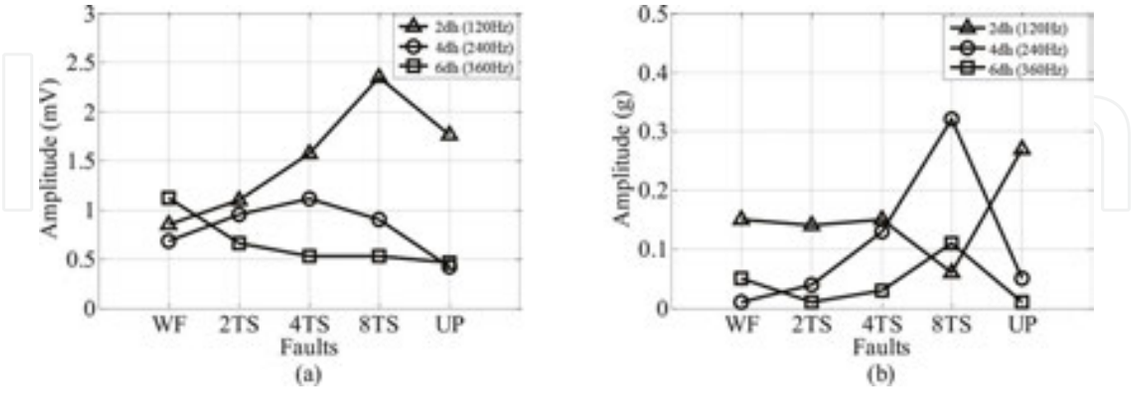

Figure 13. Tendency of the faults introduced into the motor with 80% of load, without fault (WF), two turns short (2TS), four turns short (4TS), eight turns short (8TS) and voltage unbalanced (UP): (a) magnetic flux; (b) vibration.

http://dx.doi.org/10.5772/63166

The averages of the amplitudes of the fault characteristic frequencies of the ten tests conducted under conditions without fault, two turns short circuit, four turns short circuit, eight turns short circuit, and voltage unbalanced using Hilbert transform.

4. Conclusion

A good start of any reliable diagnosis method is an understanding of the electric, magnetic, and mechanical behavior of the machine in healthy and under fault conditions. Therefore, this chapter describes a dynamic model for asymmetric motor operating conditions. The model permits the simultaneous introduction of electrical faults (stator interturn short circuit, broken rotor bars, and/or voltage unbalance) and/or mechanical faults (unbalance, mixed eccentricity, and/or shaft misalignments) for three-phase induction motors, and further detection of a specific fault in a mixture of patterned fault signs.

Further simulations are carried out to check the validation of these computational models. Then, a strategy to detect and diagnose faults is presented and tested on the rig. The approach is easy to apply and all that is required is measurement of the three line currents and voltages. Therefore, it can be used in a continuous basis without interfering with normal motor operation.

In addition, the characteristic frequency of faults is analytically studied and shown in the magnetic flux and vibration signals as a nondestructive test for induction motors.

The spectral analysis after the application of the Hilbert transform makes it possible to highlight a clear way for all modulations related to considered characteristic frequency of faults, unlike the analysis of the spectra of the vibration and magnetic flux in its raw form applying only the fast Fourier transform.

The experimental results show that this methodology can be adapted for different motors and used as a nondestructive test in real predictive maintenance programs in several industries segments.

Author details

Paulo Cezar Monteiro Lamim Filho[1*], Lane Maria Rabelo Baccarini[1] and Robson Pederiva[2]

*Address all correspondence to: plamim@yahoo.com

1 Department of Electrical Engineering, Federal University of São João del Rei, São João del Rei-MG, Brazil

2 Faculty of Mechanical Engineering, Department of Integrated Systems, University of Campinas, Campinas-SP, Brazil

References

[1] Choi S. Introduction. In: Electric Machines: Modeling, Condition Monitoring, and Fault Diagnosis. 1st ed. Taylor & Francis Group; 2013, Florida, USA. pp. 1–8.

[2] Kliman GB, Koegl RA, Stein J, Endicott RD, Madden MW. Noninvasive detection of broken rotor bars in operating induction motors. IEEE Transactions on Energy Conversions. 1988;3:873–879.

[3] Nandi S, Toliyat HA, Li X. Condition monitoring and fault diagnosis of electrical machines—a review. IEEE Transactions on Energy Conversion. 2005;20(4):719–729.

[4] Siddique A, Yadava GS, Singh B. A review of stator fault monitoring techniques of induction motors. IEEE Transactions on Energy Conversion. 2005;20:106–114.

[5] Benbouzid MEH. A review of induction motors signature analysis as a medium for faults detection. IEEE Transactions on Industrial Electronics. 2000;47:984–993.

[6] Zhongming Y. A review of induction motor fault diagnosis.. In: The Third International Power Electronics and Motion Control Conference; 2000. pp. 1353–1358.

[7] Nandi S, Toliyat HA. Novel frequency-domain based technique to detect stator inter turn faults in induction machines using stator-induced voltages after switch-off. IEEE Transaction on Industry Application. 2002;38(1):101–109.

[8] Zhang P, Du Y, Habetler TG, Lu B. A survey of condition monitoring and protection methods for medium-voltage induction motors. IEEE Transaction on Industry Application. 2011;47(1):34–46.

[9] Benbouzid MEH, Kliman GB. What stator current processing-based technique to use for induction motor rotor faults diagnosis? IEEE Transaction on Energy Conversion. 2003;18:238–244.

[10] Hou L, Bergmann NW. Novel industrial wireless sensor networks for machine condition monitoring and fault diagnosis. IEEE Transaction on Instrumentation and Measurement. 2012;61(10):2787–2798.

[11] Lamim Filho PCM, Pederiva R, Brito JN. Detection of stator winding faults in induction machines using flux and vibration analysis. Mechanical Systems and Signal Processing. 2014;42:377–387.

[12] Dias CG, Chabu I. Spectral analysis using a Hall effect sensor for diagnosing broken bars in large induction motors. IEEE Transaction on Instrumentation and Measurement. 2014;63(12):2890-2902.

[13] Cabanas MF, Pedrayes F, Melero MG, García CHR, Cano JM, Orcajo GA, Norniella JG. Unambiguous detection of broken bars in asynchronous motors by means of a flux measurement-based procedure. IEEE Transaction on Instrumentation and Measurement. 2011;60(03):891–899.

[14] Climente-Alarcon V, Antonino-Daviu JA, Haavisto A, Arkkio A. Particle filter-based estimation of instantaneous frequency for the diagnosis of electrical asymmetries in induction machines. IEEE Transaction on Instrumentation and Measurement. 2014;63(10):2454–2463.

[15] Valles-Novo R, Rangel-Magdaleno JJ, Ramirez-Cortes JM, Peregrina-Barreto H, Morales-Caporal R. Empirical mode decomposition analysis for broken-bar detection on squirrel cage induction motors. IEEE Transaction on Instrumentation and Measurement. 2015;64(05):1118–1128.

[16] Ponci F, Monti A, Cristaldi L, Lazzaroni M. Diagnostic of a faulty induction motor drive via wavelet decomposition. IEEE Transaction on Instrumentation and Measurement. 2007;56(06):2606–2615.

[17] Cristaldi L, Faifer M, Lazzaroni M, Monti A, Toscani S. An inverter-fed induction motor diagnostic tool based on time-domain current analysis. IEEE Transaction on Instrumentation and Measurement. 2009;58(05):1454–1461.

[18] Rangel-Magdaleno JJ, Peregrina-Barreto H, Ramirez-Cortes JM, Gomez-Gil P, Morales-Caporal R. FPGA-based broken bars detection on induction motors under different load using motor current signature analysis and mathematical morphology. IEEE Transaction on Instrumentation and Measurement. 2014;63(05):1032–1040.

[19] Baccarini LMR, Menezes BR, Caminhas WM. Fault induction dynamic model suitable for computer simulation: simulation results and experimental validation. Mechanical Systems and Signal Processing. 2010;24(1):300–311.

[20] Cunha CCM, Lyra ROC, Filho BC. Simulation and analysis of induction machines with rotor asymmetries. IEEE Transactions on Industry Applications. 2005;41(1):18–24.

[21] Pillay P, Hofmann P, Manyage M. Derating of induction motors operating with a combination of unbalanced voltages and over or undervoltages. IEEE Transactions on Energy Conversion. 2002;17(4):485–490.

[22] Wang YJ. An analytical study on steady state performance of an induction motor connected to unbalanced three-phase voltage. In: Power Engineering Society Winter Meeting; 2000, Singapore. pp. 159–164.

[23] Gojko MJ, Penman J. The detection of inter-turn short circuits in the windings of operating motors. IEEE Transaction on Industrial Electronics. 2000;43(5):1078–1084.

[24] Gupta BY, Culbert IM. Assessment of insulation condition in rotating machine stators. IEEE Transaction on Energy Conversion. 1993;7(3):500–505.

[25] Wiese RS, Schagginger M, Kral C, Pirker F. The integration of machine fault detection into an indirect field oriented induction machine drive control scheme—The Vienna monitoring method. In: Industry Application Conference. Thirty-Third IAS; 1998, Saint Louis. pp. 278–285.

[26] Baccarini LMR, Tavares PB, Menezes BR, Caminhas WM. Sliding mode observer for on-line broken rotor bar detection. Electric Power Systems Research. 2010;80(9):1089–1095.

[27] Bottura CP, Silvino JL, Resende P. A flux observer for induction machines based on a time-variant discrete model. IEEE Transaction on Industry Application. 1993;29(5):343–353.

[28] Batista FB, Lamim Filho PCM, Pederiva R, Silva VAD. An empirical demodulation for electrical fault detection in induction motors. IEEE Transactions on Instrumentation and Measurement. 2016;PP(99):1–11.

[29] Feldman M. Hilbert transform in vibration analysis. Mechanical Systems and Signal Processing. 2011;25:735–802.

IntechOpen